FlowSculpt: software for efficient design of inertial flow sculpting devices

Supplementary Information

Daniel Stoecklein,[‡b] Michael Davies[‡a], Joseph de Rutte[b], Chueh-Yu Wu[b],
Dino Di Carlo[*b], Baskar Ganapathysubramanian[*a]

This supplementary file contains information pertaining to the design and fabrication of the microfluidic devices described in the main text, including designs, per-pillar flow sculpting images, and some fabrication error analysis. We also include some experimental results for multi-material design using polymer precursors with varying viscosity.

Table S1 shows a table pillar indices describing each pillar diameter, location, and height available in FlowSculpt's library of pre-computed flow deformations.

Figs. S1-S6 show the per-pillar flow images for the devices from the main text, and have device designs referencing Table S1 within their captions. These images are stitched together as movies in SV01-SV06. Note that the inter-pillar distances in the pillar sequence design images are not to scale, and have been adjusted (with closer inter-pillar spacing) to be more easily viewed here. The true inter-pillar spacing used in the experiments is $\approx 10w$, for channel width w.

Fig. S7 contains error analysis on the difference between predictions of sculpted flow (using the forward model) and the flow shapes shown in experiments (using confocal microscopy).

Fig. S8 Shows additional FlowSculpt search results for the 26 letters of the Roman alphabet, using $h/w = \{0.5, 1.0\}$.

Fig. S9 Shows a test of two different materials (poly (ethylene glycol) diacrylate and poly (propylene glycol) diacrylate) in multi-material flow sculpting.

[a] *Department of Mechanical Engineering, Iowa State University, Ames, Iowa, USA. E-mail: baskarg@iastate.edu*

[b] *Department of Bioengineering, University of California, Los Angeles, California, USA. E-mail: dicarlo@ucla.edu*

‡ These co-first authors contributed equally to this work.

∗ Corresponding authors.

		Pillar diameter (d/w)						Pillar height (h_p/h)
		0.375	**0.500**	**0.625**	**0.750**	**0.875**	**1.000**	
Pillar location (y/w)	**-0.375**	0	8	16	24			**1.0**
	-0.250	1	9	17	25			
	-0.125	2	10	18	26			
	0.000	3	11	19	27			
	0.125	4	12	20	28			
	0.250	5	13	21	29			
	0.375	6	14	22	30			
	0.500	7	15	23	31			
	-0.375	32	40	48	56	64	72	**0.5**
	-0.250	33	41	49	57	65	73	
	-0.125	34	42	50	58	66	74	
	0.000	35	43	51	59	67	75	
	0.125	36	44	52	60	68	76	
	0.250	37	45	53	61	69	77	
	0.375	38	46	54	62	70	78	
	0.500	39	47	55	63	71	79	

Table S1: Each pillar of diameter d/w, location y/w, and height h_p/h (normalized to the microchannel width w and height h.) maps onto an integer index (0-79).

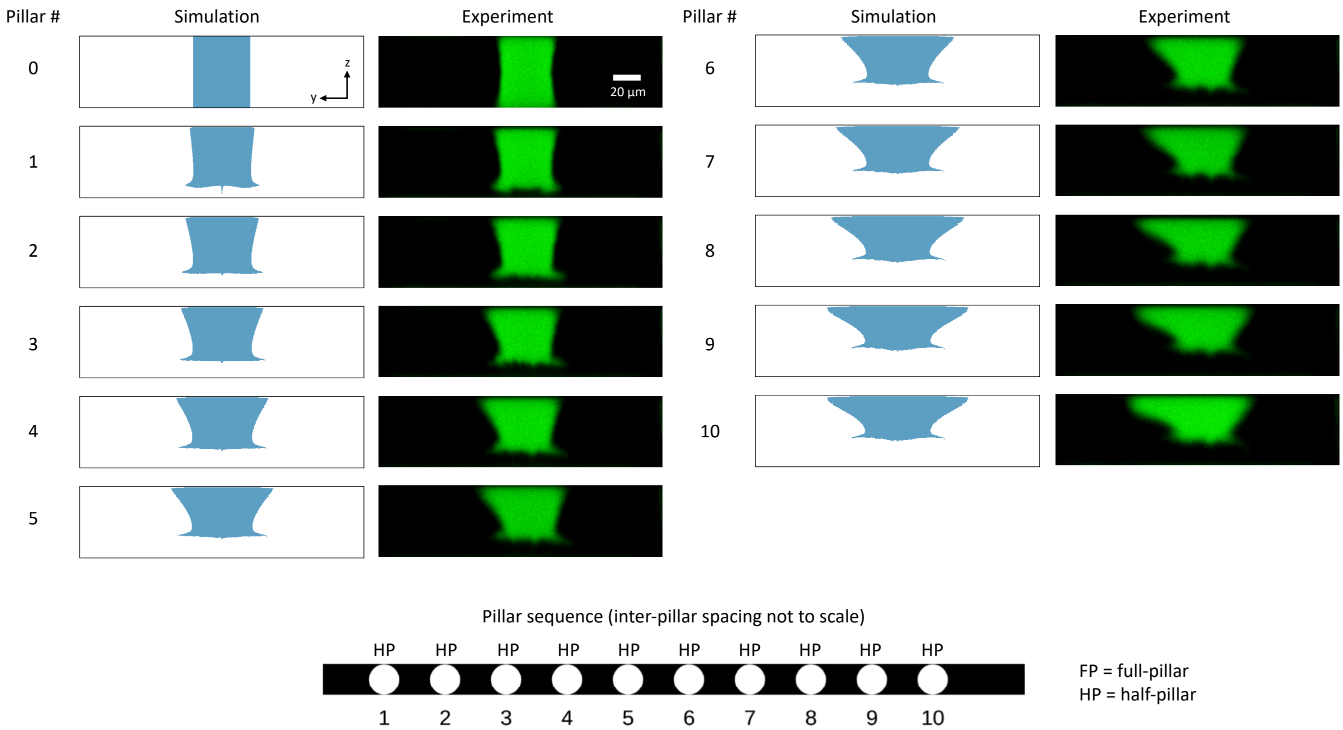

Figure S1: Per-pillar images showing the development of the 10-pillar sequence using only $d/w = 1.0$, $y/w = 0.0$ half-pillars. Pillar sequence: [75, 75, 75, 75, 75, 75, 75, 75, 75, 75]. Inlet flow pattern: widths=[0.4, 0.2], materials=[0,1,0].

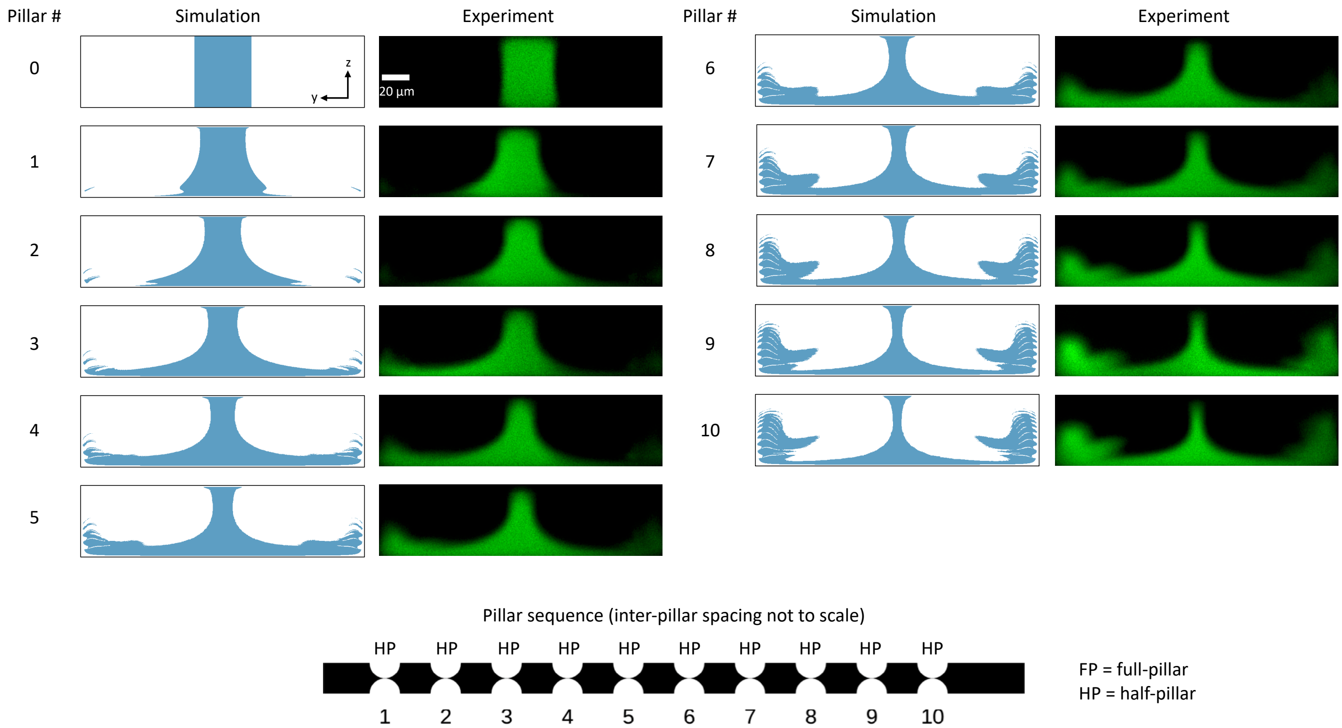

Figure S2: Per-pillar images showing the development of the 10-pillar sequence using only $d/w = 1.0$, $y/w = 0.5$ half-pillars. Pillar sequence: [79, 79, 79, 79, 79, 79, 79, 79, 79, 79]. Inlet flow pattern: widths=[0.4, 0.2], materials=[0,1,0].

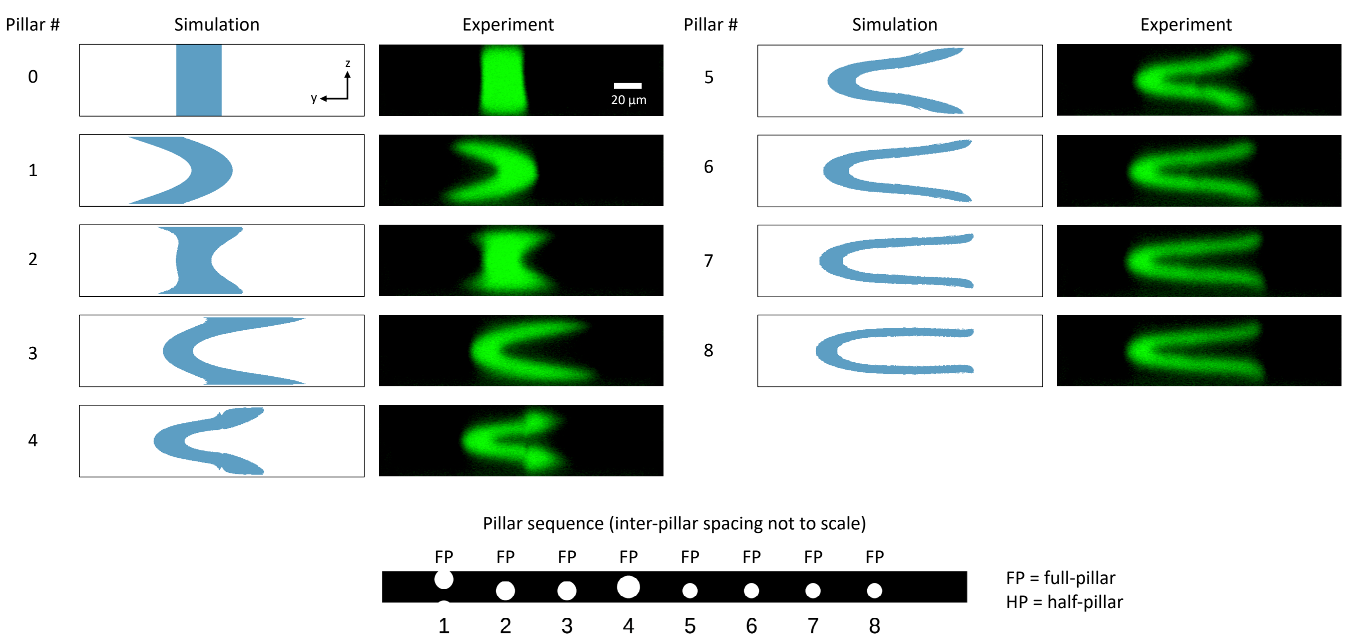

Figure S3: Per-pillar images showing the development of the the “U” flow shape. Pillar sequence: [21, 18, 18, 27, 10, 10, 10, 10]. Inlet flow pattern: widths=[0.34, 0.16], materials=[0, 1, 0].

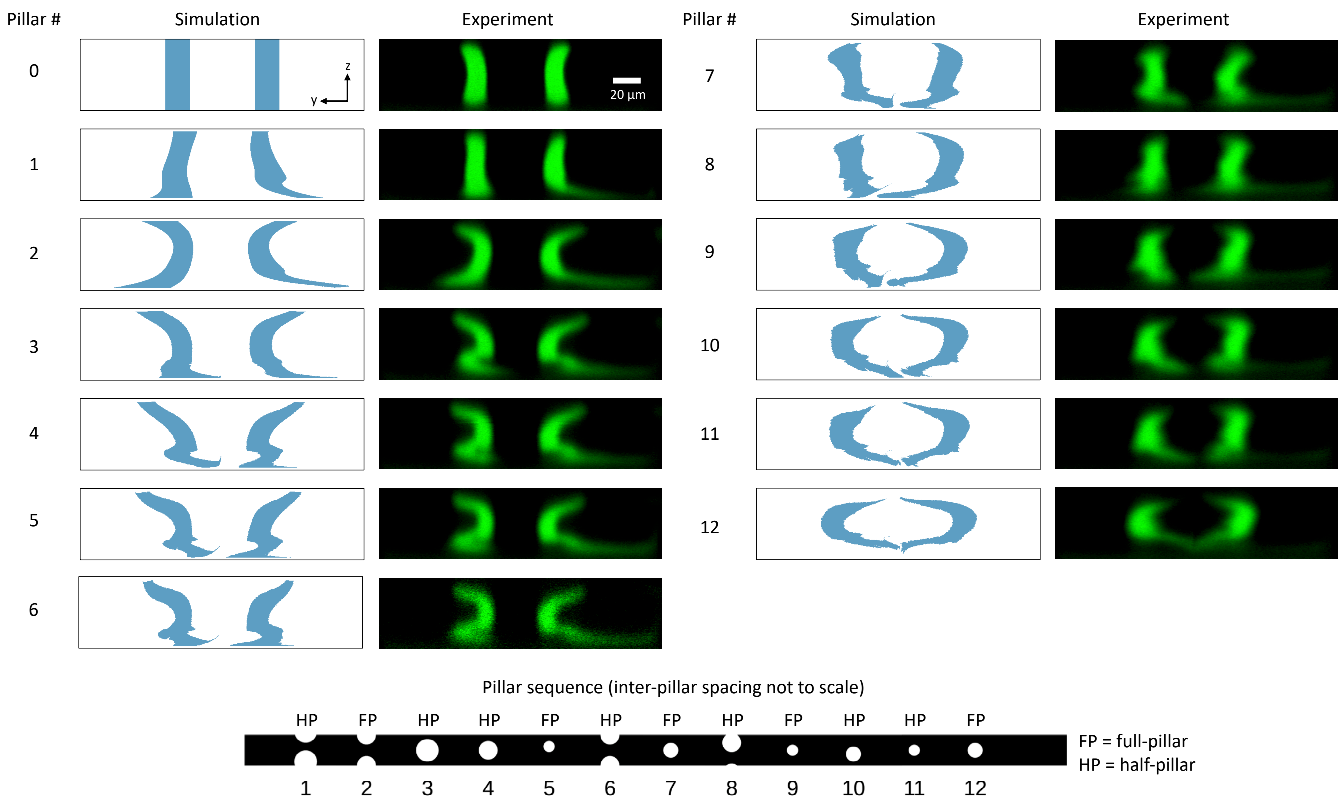

Figure S4: Per-pillar images showing the development of the the "C" flow shape. Pillar sequence: [56, 23, 59, 51, 36, 55, 11, 53, 3, 42, 35, 11]. Inlet flow pattern: widths=[0.3, 0.086, 0.23, 0.086], materials=[0, 1, 0, 1, 0].

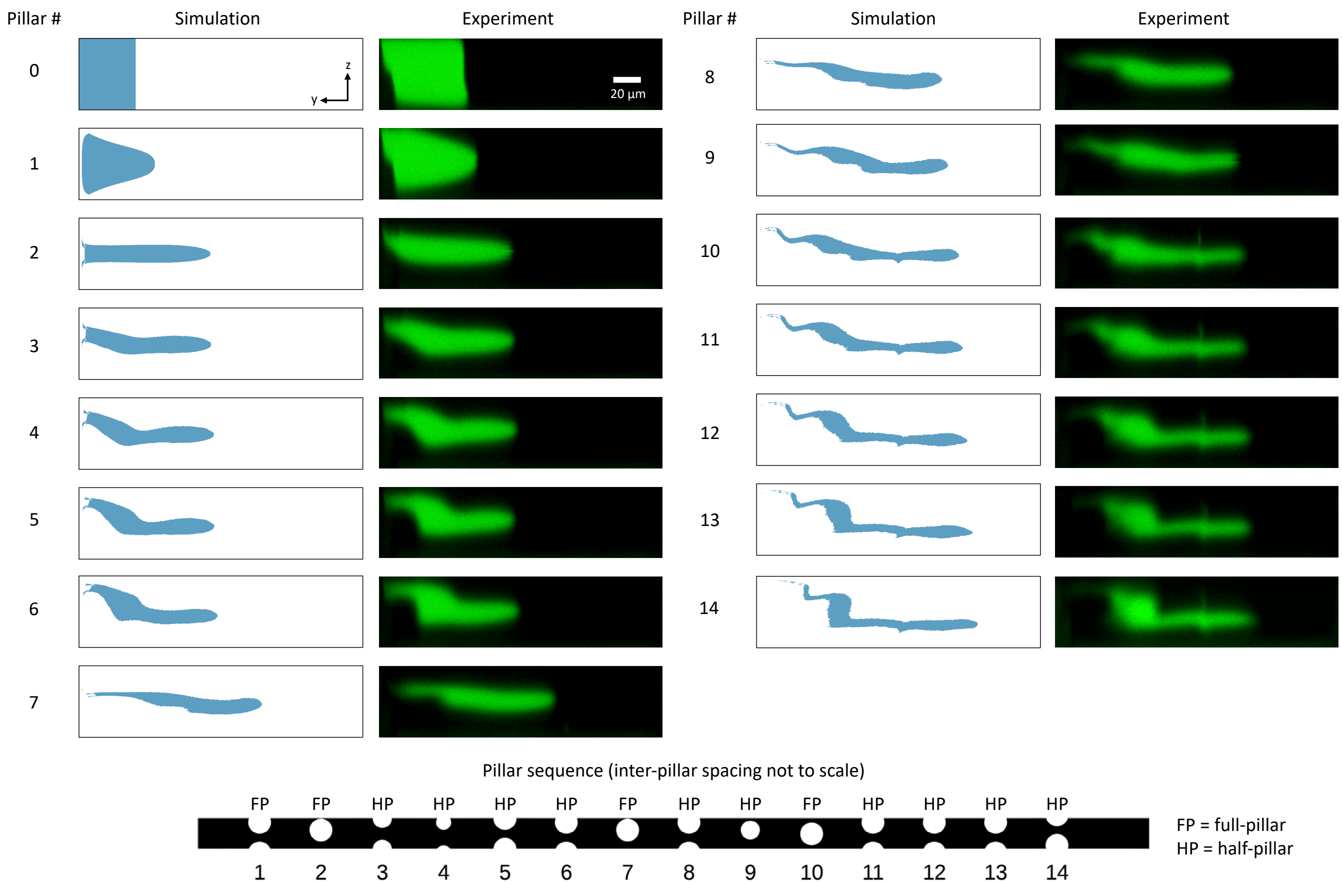

Figure S5: Per-pillar images showing the development of the the “L” flow shape. Pillar sequence: [30, 28, 55, 46, 63, 62, 28, 62, 52, 27, 62, 62, 62, 56]. Inlet flow pattern: widths=[0.2], materials=[1, 0].

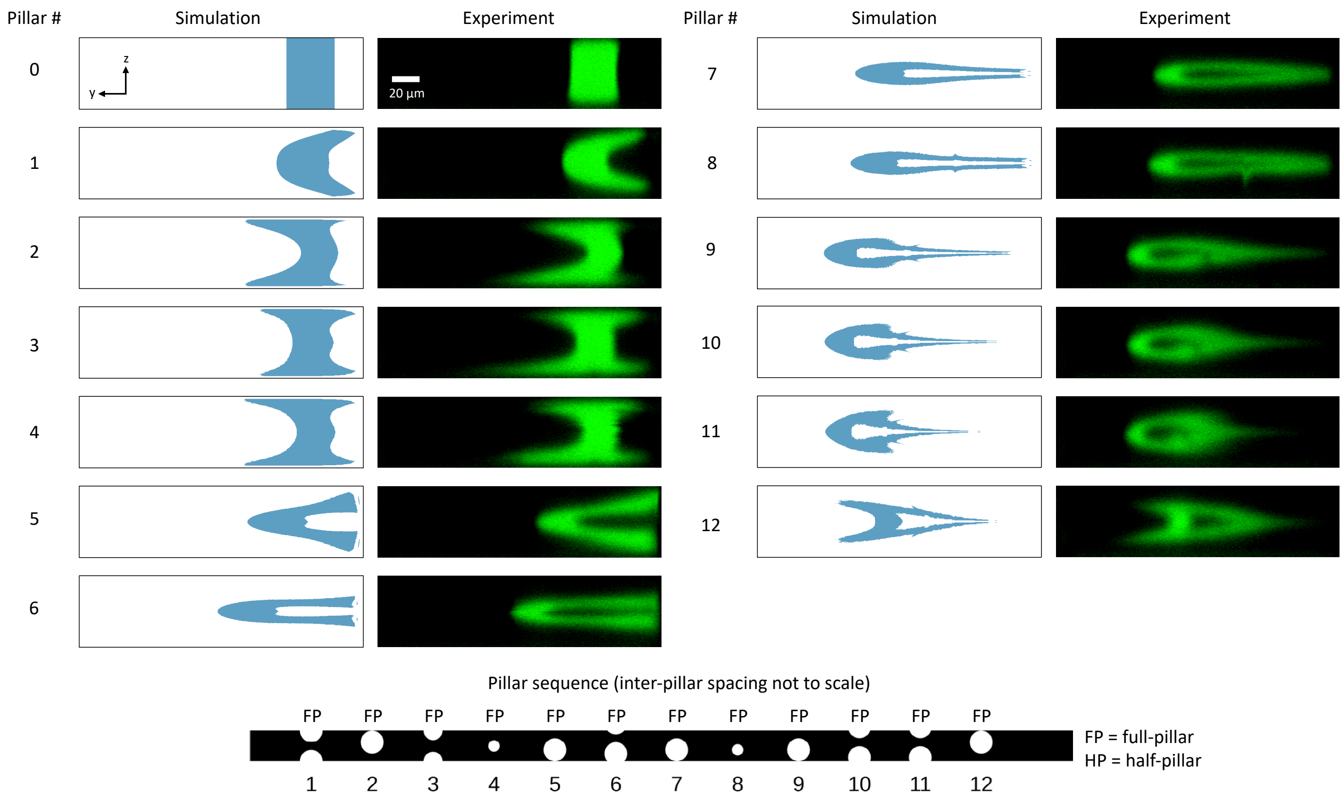

Figure S6: Per-pillar images showing the development of the the "A" flow shape. Pillar sequence: [31, 28, 23, 3, 26, 25, 26, 2, 26, 24, 24, 28]. Inlet flow pattern: widths=[0.73, 0.17], materials=[0,1,0].

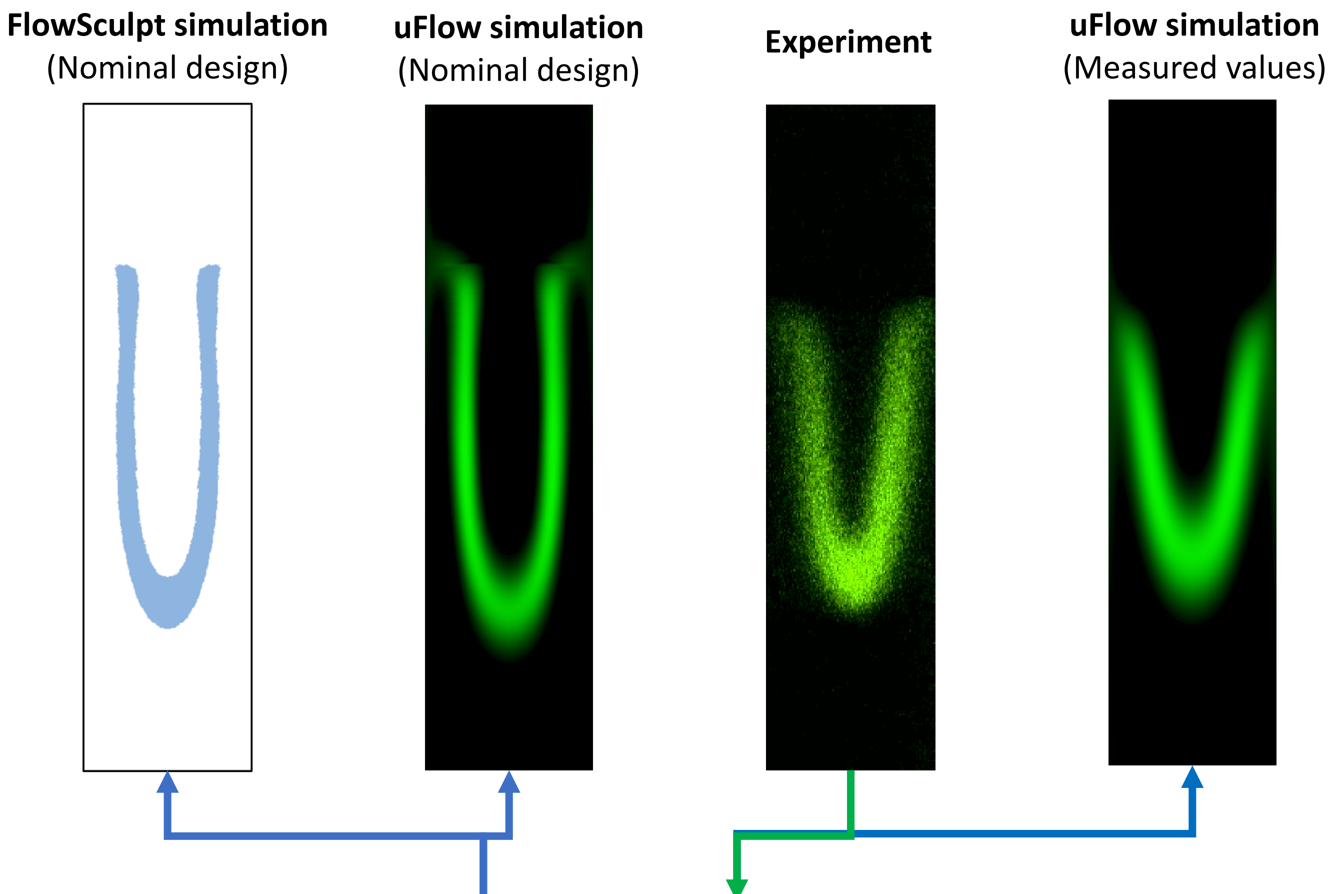

Pillar index	Design (μm)	Measured (μm)	Relative error (%)
1	62.5	51.4	**-17.8**
2	62.5	53.9	**-13.7**
3	62.5	51.5	**-17.5**
4	75.0	64.6	**-13.8**
5	50.0	38.2	**-23.6**
6	50.0	38.1	**-23.8**
7	50.0	38.5	**-23.1**
8	50.0	38.9	**-22.2**

Figure S7: We use the uFlow software (www.biomicrofulidics.com/software.php) to verify that errors in fabrication, specifically undersized pillar structures, are primarily responsible for differences between flow sculpting predictions and experiment. In the first two flow images shown above, FlowSculpt and uFlow both predict a similar flow shape (intended to resemble the letter "U") from the designed pillar sequence in the table below, with uFlow's diffusion model introducing some slight differences. After fabricating the device, confocal images showed a significant departure from the nominal design (shown in the third image from the left). Measurements of each pillar's diameter (which is known to be the most sensitive parameter pertaining to flow sculpting [1]) revealed that all pillars were significantly undersized, with relative error between 13% and 24% (shown in table S1). We used uFlow's interpolative advection library [2] to simulate the as-fabricated device using the measured values for each pillar diameter, with the resulting flow shape prediction showing excellent agreement with the confocal image. Thus, we attribute significant differences between predicted and observed flow shapes to errors that occur in fabrication, primarily related to undersized pillar diameters.

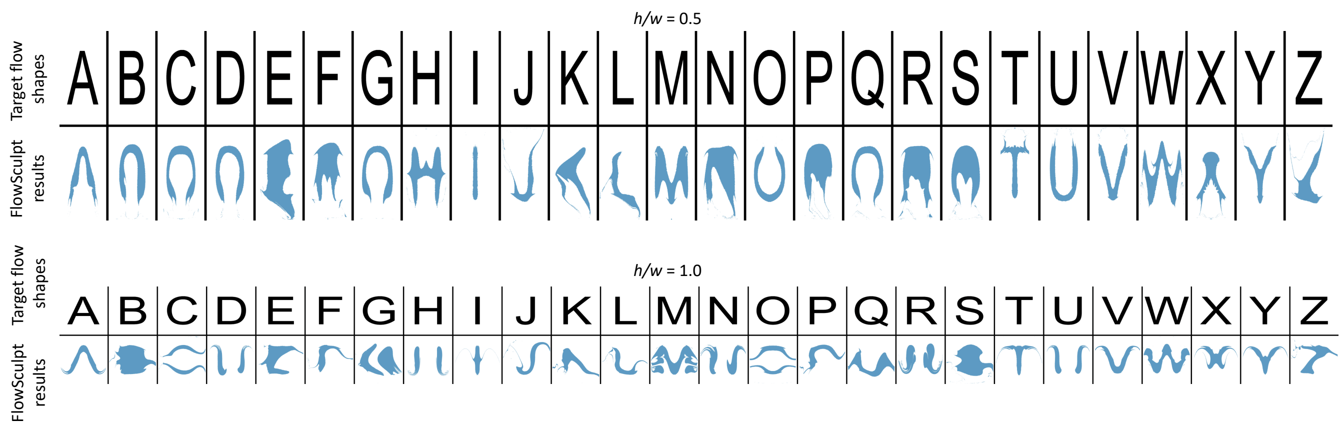

Figure S8: Additional search results for the 26 letters of the Roman alphabet using aspect ratios $h/w = \{0.5, 1.0\}$, and $Re = \{10, 20, 30, 40\}$. The apparently less-capable design spaces at these aspect ratios are possibly due to the weakened vorticity generated at the surface of the pillar and where the pillar meets the channel walls. As the channel aspect ratio becomes larger, these combined sources of vorticity become more separated, making potentially more complex, but weaker flow deformations.

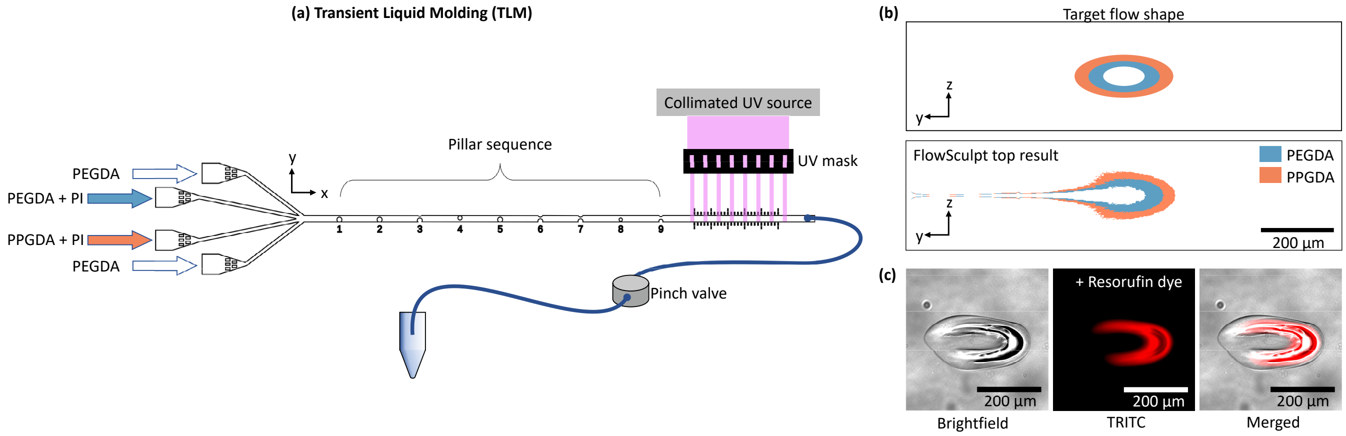

Figure S9: (a) We used transient liquid molding [3] (TLM) to test multi-material flow sculpting with two different co-flowing materials: poly (ethylene glycol) diacrylate (PEGDA; $M_n \sim 575$; 437441, Sigma-Aldrich) and poly (propylene glycol) diacrylate (PPGDA; $M_n \sim 800$; 445024, Sigma-Aldrich)), blending each material with ethanol (60/40 PEGDA/ethanol, 90/10 PPGDA/ethanol) to match their densities to avoid issues with buoyancy. However, viscosity was not matched, with measured blend viscosities of 6.99 mPa s (PEGDA) and 52.32 mPa s (PPGDA). (b) A multi-material flow design was created using FlowSculpt, targeting a nested 2-material flow shape. We used a modified version of our in-house microparticle fabrication technique TLM [3] to create 3D microparticles by adding 2-hydroxy-2-methylpropiophenone as a photoinitiator to adjacent PEGDA and PPGDA flow streams in a 1200 µm x 300 µm channel. The resulting microparticles were washed in DPBS solution ($10^{-}3$ pluronic) with fluorescent resorufin (TCI-R0012, TCI Chemicals), which should be absorbed into the hydrophillic PEGDA layer of the microparticles, but not the hydrophobic PPDGDA layer. (a) A microparticle is imaged using brightfield and fluorescent microscopy, showing that the two different polymer materials largely reflected the flow shape design, despite their varying viscosity. The increase in particle size from 240 µm x 135 µm (designed) to 300 µm x 170 µm (measured) is likely due primarily to mass diffusion of the two materials and the photoinitiator during the flow stoppage (1.0 s) and UV curing time (500 ms), while we attribute the top-bottom asymmetry to weak UV illumination from our collimated UV source, which was placed ≈15 cm from the microchannel for ease of alignment during fabrication. While this experiment shows that some mismatch in fluid properties is allowed (viscosity, in this case), results will certainly vary depending on how large the disparity, and which properties remain matched.

References

[1] Hamed Amini, Elodie Sollier, Mahdokht Masaeli, Yu Xie, Baskar Ganapathysubramanian, Howard A Stone, and Dino Di Carlo. Engineering fluid flow using sequenced microstructures. *Nature Communications*, 4(May):1826, jan 2013.

[2] Daniel Stoecklein, Keegan Owsley, Chueh-Yu Wu, Dino Di Carlo, and Baskar Ganapathysubramanian. uFlow: software for rational engineering of secondary flows in inertial microfluidic devices. *Microfluidics and Nanofluidics*, 22(7):74, jun 2018.

[3] Chueh Yu Wu, Keegan Owsley, and Dino Di Carlo. Rapid Software-Based Design and Optical Transient Liquid Molding of Microparticles. *Advanced Materials*, 27(48):7970–7978, 2015.